Front. Phys., 2012, 7(4): 399–407
DOI 10.1007/s11467-011-0210-3

REVIEW ARTICLE

Synthesis, microstructures, and magnetoelectric couplings of electrospun multiferroic nanofibers

Shu-Hong Xie (谢淑红)[1,2,*], **Yun-Ya Liu** (刘运牙)[1], **Jiang-Yu Li** (李江宇)[2,†]

[1] *Faculty of Materials, Optoelectronics and Physics, and Key Laboratory of Low Dimensional Materials & Application Technology of Ministry of Education, Xiangtan University, Xiangtan 411105, China*

[2] *Department of Mechanical Engineering, University of Washington, Seattle, WA 98195, USA*

*E-mail: * shxie@xtu.edu.cn, † jjli@uw.edu*

Received July 20, 2011; accepted August 18, 2011

Multiferroic materials with two or more types of ferroic orders have attracted a great deal of attention in the last decade for their magnetoelectric coupling, and new ideas and concepts have been explored recently to develop multiferroic materials at nano-scale. Motivated by theoretical analysis, we synthesized single-phase $BiFeO_3$ (BFO) nanofibers, $Pb(Zr_{0.52}Ti_{0.48})O_3$-$CoFe_2O_4$ (PZT-CFO) and $Pb(Zr_{0.52}Ti_{0.48})O_3$-$NiFe_2O_4$ (PZT-NFO) composite nanofibers, and $CoFe_2O_4$-$Pb(Zr_{0.52}Ti_{0.48})O_3$ (CFO-PZT) core-shell nanofibers using sol-gel based electrospinning. These nanofibers typically have diameters in the range of a few hundred nanometers and grain size in the range of 10s nanometers, and exhibits both ferroelectric and ferromagnetic properties. Piezoresponse force microscopy (PFM) based techniques have also been developed to examine the magnetoelectric coupling of the nanofibers, which is estimated to be two orders of magnitude higher than that of thin films, consistent with our theoretical analysis. These nanofibers are promising for a variety of multiferroic applications.

Keywords multiferroic, nanofiber, magnetoelectric, piezoresponse force microscopy

PACS numbers 75.30.Kz, 75.80.+q

Contents

1 Introduction

Multiferroic materials with two or more types of ferroic orders have attracted a great deal of attention in the last decade [1–5]. In particular, the coexistence of electric and magnetic ordering makes it possible to manipulate the electric state of a multiferroic material through a magnetic field, or vice versa, and thus opens door for a variety of applications [6–10], including multiple-state memory devices that can be electrically written and magnetically read, electrically controlled microwave phase shifters or ferromagnetic resonance devices, magnetically controlled electro–optic or piezoelectric devices, and broadband magnetic field sensors. Nevertheless, the magnetoelectric couplings in single-phase multiferroic materials are usually extremely small [1], and much of the attention has been focused on developing hybrid multiferroic composites consisting of ferroelectric and ferromagnetic phases [11–18], wherein the magnetoelectric coupling is induced indirectly through the interactions of piezoelectric and magnetostrictive effects, the so-called product property. An excellent survey of literature in this regard can be found in a recent review article [19].

In recent years, new ideas and concepts have also been explored to develop multiferroic materials at nanoscale, including multiferroic nanoparticles [20–22], heterostruc-

tured thin films [23–26], and solid solutions [27–29], which promise much tighter coupling between ferroelectric and ferromagnetic phases, and offer additional degrees of freedom in size, interface and epitaxial strain to further enhance the magnetoelectric coupling. Among all possible multiferroic nanostructures, one-dimensional nanofibers are particularly fascinating. It could not only reveal interesting one-dimensional multiferroicity at nanoscale, but could also enable novel multiferroic devices, such as a one-dimensional magnetoelectric probe with nanometer resolution. In addition, the constraint of the substrate on the nanofibers could be substantially relaxed compared to more conventional form of thin films, and thus allows maximum demonstration of intrinsic magnetoelectric coupling without the substrate clamping. The large aspect ratio of the nanofibers also makes it possible to magnify the mechanical displacement due to the piezoelectric or magnetostrictive effect, and thus enhance the magnetoelectric coupling even further. In the past four years, our group has pioneered the analysis [30], synthesis, and characterizations of multiferroic nanofibers [31–34], which will be reviewed here.

2 Theoretical analysis

A multiferroic composite nanofiber consisting of a ferroelectric phase $Pb(Zr_{0.52}Ti_{0.48})O_3$ (PZT) and a ferromagnetic phase $CoFe_2O_4$ (CFO) aligned and electrically poled along x_1 axis has been analyzed using beam theory [30]. When a quasi-static magnetic field is applied either along or perpendicular to the axis of nanofiber, the strain from the magnetostrictive effect of CFO is blocked due to the mechanical constraint when both ends are assumed to be fixed, inducing internal stress in the fiber that results in electric charge from the piezoelectric effect of PZT. This leads to normalized magnetoelectric coupling coefficient

$$r_{1k} = \sqrt{\frac{\varepsilon_0}{\mu_0}} \frac{d_{11} q_{k1}}{\kappa_{11} S_{11} - d_{11}^2} \tag{1}$$

where ε_0 and μ_0 are permittivity and permeability of vacuum, d_{11} is the piezoelectric coefficient of PZT, q_{k1} is the piezomagnetic coefficient of CFO, and κ_{11} and S_{11} are dielectric constant and elastic compliance of the composite nanofiber. Similar analysis has also been carried out for multiferroic thin film of similar compositions, and the transverse magnetoelectric coefficients of nanofiber and thin film are compared, as shown in Fig. 1(a). It is observed that the composite nanofiber exhibit the highest magnetoelectric coupling at 50% of PZT, and its value is two orders of magnitude higher than that of composite thin film. Furthermore, the magnetoelectric coupling can be magnified by driving the nanofiber near its mechanical resonance, and the dynamic analysis suggests that the frequency dependent magnetoelectric coefficient under free-end boundary condition is given by

$$r_{1k} = \sqrt{\frac{\varepsilon_0}{\mu_0}} \frac{d_{11} q_{k1}}{\kappa_{11} S_{11} - d_{11}^2} \left[\frac{\cos(kx_1)}{\cos(kL)} - 1 \right] \tag{2}$$

which is clearly maximized at mechanical resonance when $\cos(kL) = 0$, where k is the wave number. A comparison of the dynamic magentoelectric coefficient between the nanofiber and thin film is shown in Fig. 1(b), with volume fraction of PZT set to be 25% and loss tangent set to be 5%. It is observed that the dynamic magnetoelectric coefficient is about two orders of magnitude higher than the corresponding static one, and that of nanofiber is about one order of magnitude higher than that of thin film. These analyses established the superior magnetoelectric coupling in multiferroic nanofibers compared to multiferroic thin films of similar compositions.

3 Electrospinning of nanofibers

A variety of techniques have been developed to synthesize one-dimensional nanostructures such as nanowires and nanofibers, including phase separation [35, 36], template synthesis [37, 38], hydrothermal process [39, 40], evaporation [41, 42], electrodeposition [43, 44], and

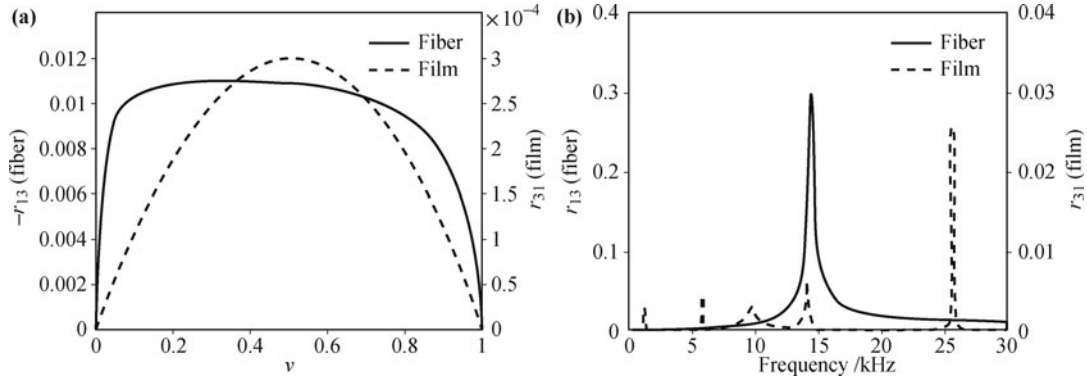

Fig. 1 The magnetoelectric coefficients of multiferroic PZT-CFO composite nanofiber, in comparison with multiferroic thin film of similar composition: **(a)** static coefficient versus the volume fraction of PZT; and **(b)** dynamic coefficient versus the driving frequency, with the volume fraction of PZT set to be 25%. Reproduced from Ref. [30], Copyright © 2009 American Institute of Physics.

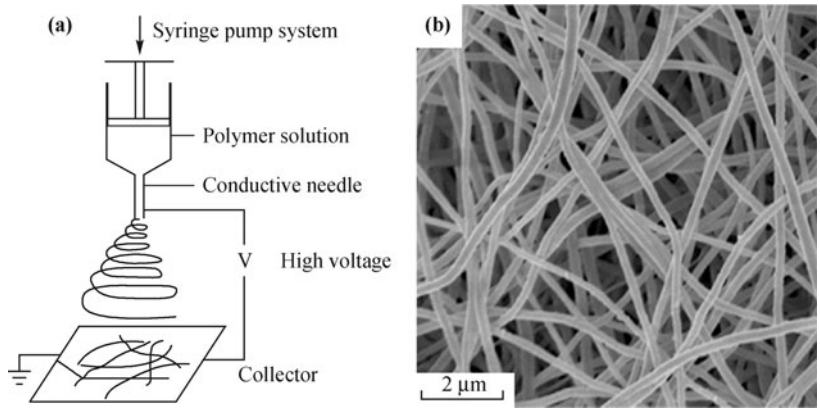

Fig. 2 Electrospinning of nanofibers: **(a)** the schematic of overall process; and **(b)** typical nanofibers synthesized by electrospinning in our lab.

electrospinning [45, 46], and multiferroic composite nanowire has indeed been synthesized by template synthesis combined with electrodeposition [44]. In this review, however, we focus on electrospinning of multiferroic nanofibers, instead, that we have been working on since 2007.

Electrospinning is a versatile technique that has been applied to synthesize a wide range of polymeric [47, 48], ceramic [49], composite [50], and core-shell [51] nanofibers. The term is derived from "electrostatic spinning", wherein the formation of nanofibers is accomplished through the uniaxial stretching of a viscoelastic solution induced by electrostatic forces. The principle, operations, and applications of electrospinning can be found in several excellent review articles that the readers can refer to [47–49, 52–55], and here we only briefly introduce the basic concept.

A typical electrospinning set-up consists of three components including a syringe pump that drives polymer solution through the metallic needle, a high voltage supplier that is connected to the metallic needle, and a metallic collector that is grounded, as schematically shown in Fig. 2(a). At a sufficient high voltage, the repulsive electrostatic forces within the charged solution can overcome the surface tension of the solution, which forms a Taylor cone at the tip of the needle and causes the ejection of a thin jet from the tip of the Taylor cone [47]. Although the jet is stable near the tip of the spinneret, it soon enters a bending instability stage with further stretching of the solution jet under the electrostatic forces as the solvent evaporates, resulting in the formation of continuous nanofibers collected by the grounded collectors. A scanning electron microscopy (SEM) image of typical nanofibers synthesized in our lab is shown in Fig. 2(b), with nanofiber diameters range from 100 to 300 nm. In general, the morphology and size of nanofibers can be controlled by processing parameters, including solution concentration and viscosity, electric field strength, and collecting distance [56]. While the process was originally developed for polymer nanofibers, ceramic and composite nanofibers have also been successfully synthesized by combining sol-gel process with electrospinning, followed by appropriate heat treatment [47, 57].

In addition to solid nanofibers, coaxial electrospinning has also been developed to synthesize core-shell type and hollow nanofibers [50, 51, 58], as shown in Fig. 3. The overall setup is schematically shown in Fig. 3(a), along with the detailed configuration of coaxial spinneret and the expected cross section of core-shell nanofiber. The image of actual coaxial spinneret is shown in Fig. 3(b). It consists of two commercial blunt needles with different diameters and lengths that are assembled into a coaxial structure. During the electrospinning process, the syringe loaded with one type of solution is connected vertically to the inside needle as the material for core, and the syringe loaded with another type of solution is connected horizontally to the outside needle as the material for shell, resulting in a core-shell type of configuration. If the core can be burned off, leaving behind a structure with only the shell, then hollow nanofibers can also be obtained.

4 Multiferroic nanofibers by electrospinning

In the past few years, we have synthesized a variety of single-phase [33], composite [31, 32], and core-shell type [34] multiferroic nanofibers by electrospinning in combination with sol-gel process, which will be briefly reviewed next.

4.1 Ultrafine $BiFeO_3$ fibers

$BiFeO_3$ (BFO) is one of the most studied single-phase multiferroic material, thanks to its multiferroic properties and magnetoelectric coupling at room temperature [59]. Ultrafine BFO fibers have been synthesized by electrospinning in our lab as detailed in Ref. [33]. The BFO precursors were prepared first, then poly(vinyl pyrrolidone) (PVP) were added to the BFO precursor solution directly and stirred continuously to form homogeneous

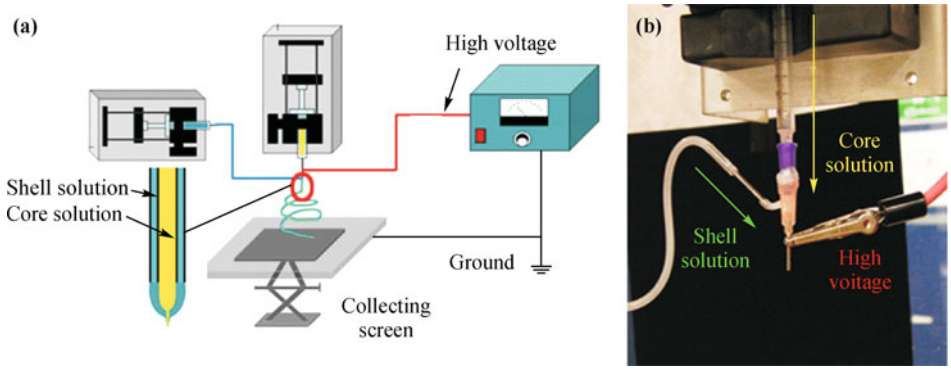

Fig. 3 Coaxial electrospinning of core-shell type nanofibers: **(a)** the schematics of the setup; and **(b)** the photo of actual coaxial spinneret. Reproduced from Ref. [34], Copyright © 2011 Royal Society of Chemistry.

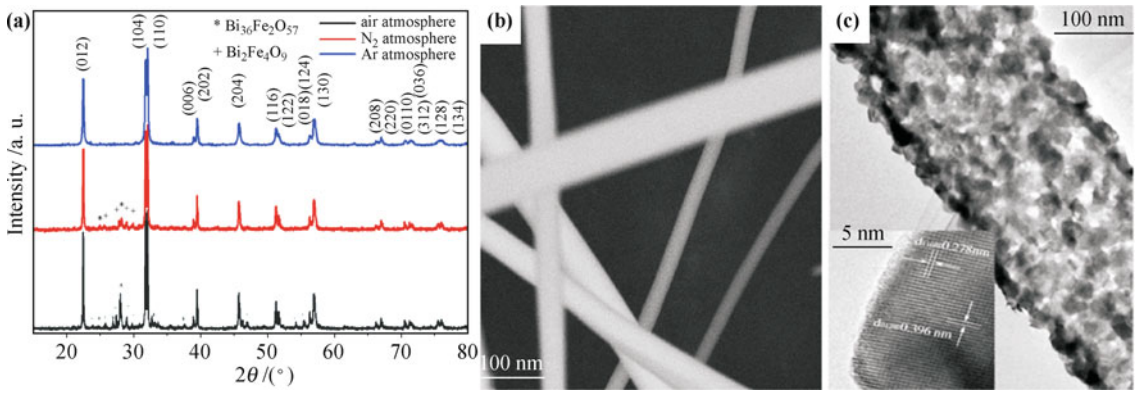

Fig. 4 Structure of ultrafine BFO fibers: **(a)** XRD pattern under different atmospheres; **(b)** SEM image of calcined fiber; and **(c)** TEM image of etched fiber with HRTEM image in the inset. Reproduced from Ref. [33], Copyright © 2008 American Institute of Physics.

electrospinning solutions. The solutions were electrospun and the ultrafine fibers spun were collected, then dried and calcined in three different atmospheres. The X-ray diffractions (XRD) show excellent crystallinity of BFO fibers, as seen in Fig. 4(a). Phase pure rhombohedral perovskite BFO is obtained when Ar is used as protective atmosphere, and small amount of $Bi_{36}Fe_2O_{57}$ and $Bi_2Fe_4O_9$ impurity phases are observed when the fibers are fired in air or nitrogen atmosphere instead. The SEM image of calcined BFO fibers shown in Fig. 4(b) suggests that the diameter of calcined fibers is in the range of 100∼300 nm, with the diameter kept uniform across the fiber length. A transmission electron microscopy (TEM) image confirms that BFO fiber is composed of rather dense nanocrystalline grains with the grain size around 20 nm, as shown in Fig. 4(c). The rhombohedral perovskite structure is also confirmed by high resolution TEM (HRTEM), as shown in the inset of Fig. 4(c).

The high voltage piezoresponse force microscopy (PFM) has been carried out to verify the piezoelectricity and ferroelectricity of BFO ultrafine fibers, with PFM amplitude image in Fig. 5(a) showing clear ferroelectric domain structure. To switch the polarization in the ultrafine fiber, a sequence of DC voltage is applied, and the butterfly loop between PFM amplitude and applied voltage characteristic of ferroelectricity has been obtained, as shown in Fig. 5(b), with the coercive field of BFO fiber estimated to be around 150 MV/m, and the maximum field induced displacement measured to be around 700 pm. This establishes the ferroelectricity of the BFO fiber as non-ferroelectric materials would show no hysteresis. Furthermore, weak ferromagnetism of nanocrystalline BFO fibers is confirmed by vibrating sample magnetometer (VSM) measurement, with saturation magnetization as large as 4 emu/g and coercive field around 200 Oe observed, as shown in Fig. 5(c). Such weak ferromagnetism is believed to be caused by nanocrystalline structure of BFO fibers [60]. We made an additional attempt to measure the magnetoelectric coupling of BFO fibers without success.

4.2 $Pb(Zr_{0.52}Ti_{0.48})O_3$-$CoFe_2O_4$ and $Pb(Zr_{0.52}Ti_{0.48})O_3$-$NiFe_2O_4$ composite nanofibers

We have also synthesized multiferroic composite nanofibers by electrospinning, with ferroelectric phase being $Pb(Zr_{0.52}Ti_{0.48})O_3$ (PZT), and ferromagnetic phase being either CFO or NFO. The precursors of ferroelectric and ferromagnetic phases were mixed together with different molar ratios, and electrospun after PVP polymers were added. The nanofibers were then collected, dried, followed by appropriate heat treatment,

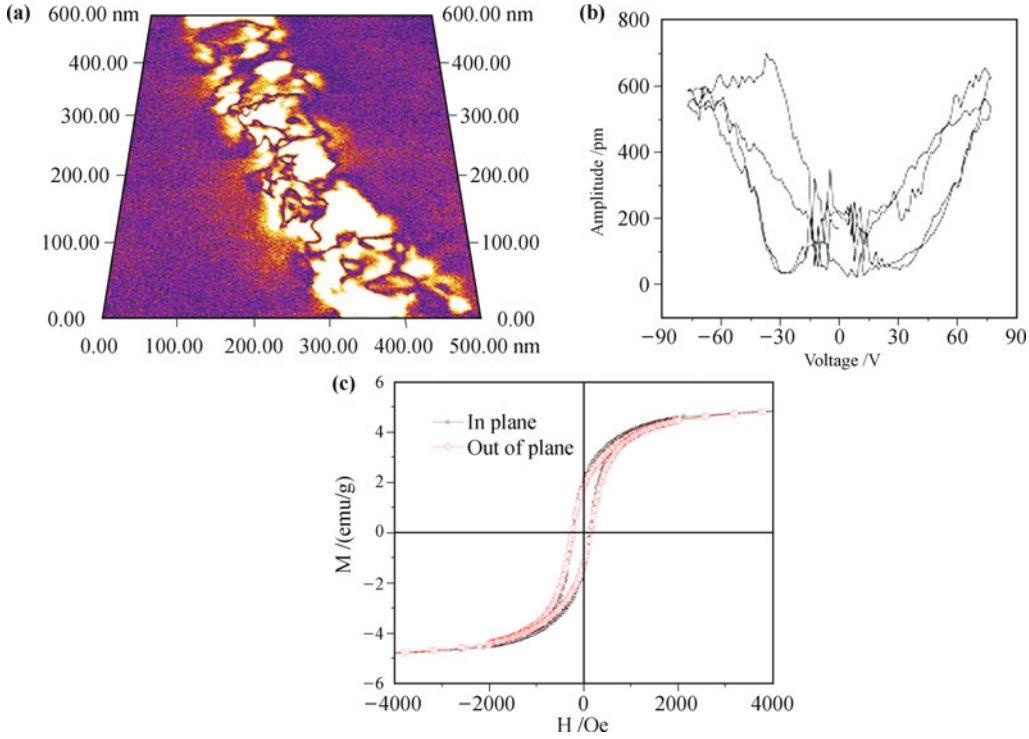

Fig. 5 Multiferroic properties of ultrafine BFO fiber: **(a)** PFM amplitude image; **(b)** PFM amplitude–voltage butterfly loop; and **(c)** VSM magnetic hysteresis loop. Reproduced from Ref. [33], Copyright © 2008 American Institute of Physics.

as detailed in Refs. [31, 32]. SEM morphologies of the composite nanofibers are similar to those of BFO, with diameters of the nanofibers ranging from 100 to 400 nm, as seen in Fig. 6(a), and the energy dispersion spectroscopy (EDS) indicates that ferroelectric and ferromagnetic species are randomly distributed, as seen in Figs. 6(b) and (c). The XRD reveals both ferroelectric pervoskite phase and ferromagnetic spinel phase, as confirmed by HRTEM in Fig. 6(d) and its inset. The grain size of the composite nanofiber is around 30 nm, slightly larger than that of BFO.

The ferroelectric properties of the composite nanofibers have been confirmed by PFM hysteresis, and their ferromagnetic properties have been measured by VSM hysteresis. The comparisons of multiferroic properties between the PZT-CFO and PZT-NFO nanofibers are summarized in Fig. 7, where it is observed that PZT-CFO nanofibers have higher piezoelectric coefficient [Fig. 7(a)], magnetization [Fig. 7(b)], and magnetic coercive field [Fig. 7(c)] than PZT-NFO nanofibers of similar compositions, probably because they have better crystallinity than PZT-NFO nanofibers.

4.3 $CoFe_2O_4$-$Pb(Zr_{0.52}Ti_{0.48})O_3$ core-shell nanofibers

The mixing of ferroelectric and ferromagnetic precursors results in composite nanofibers with random distribution of their constituent. To overcome this shortcoming, we synthesized CFO-PZT core-shell nanofibers by coaxial electrospinning, as schematically shown in Fig. 3. The preparations of PZT and CFO precursors were similar to PZT-CFO composite nanofiber, except that polymethyl

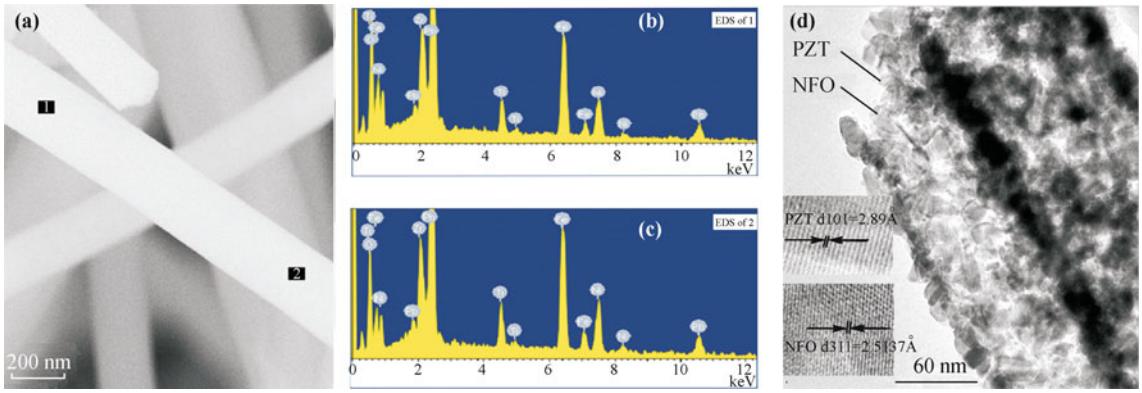

Fig. 6 SEM **(a)**, EDS **(b, c)** and TEM **(d)** images of PZT-NFO composite nanofibers with molar ratio 1:1. Reproduced from Ref. [32], Copyright © 2008 American Institute of Physics.

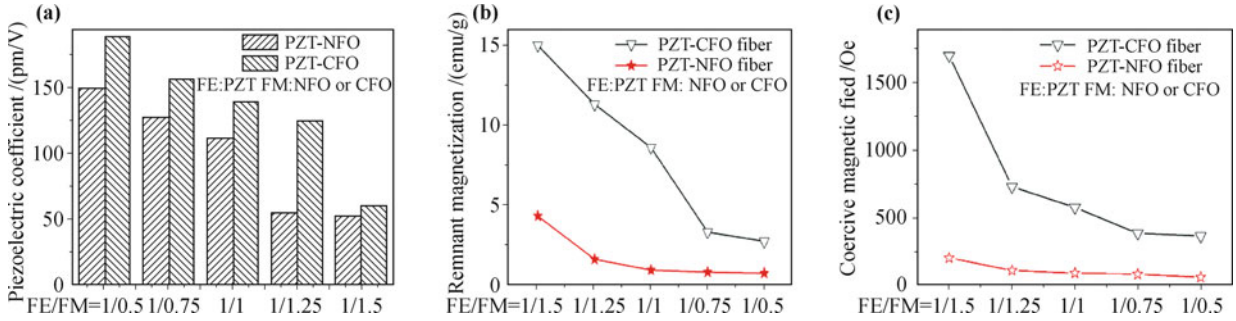

Fig. 7 The comparison between PZT-NFO and PZT-CFO nanofibers of identical PZT concentration: **(a)** piezoelectric coefficients; **(b)** remnant magnetization and **(c)** coercive magnetic field.

methacrylate (PMMA) was used as polymers instead of PVP. During the electrospinning process, the syringe loaded with CFO precursor was connected vertically to the inside 22-gauge needle as a solution for the core, and the syringe loaded with PZT precursor was connected horizontally to the outside 18-gauge needle through the drilled hole as a solution for the shell. The morphology of CFO-PZT core-shell nanofibers is shown in Fig. 8. The typical cross section SEM image of the nanofibers is given in Fig. 8(a), and fibrous core-shell structures with diameters in the range of 100 to 500 nm are observed. The detailed cross-sections of three nanofibers are shown in Fig. 8(b), where it is observed that the CFO core is relatively porous, while PZT shell is relatively dense, and some gaps exist at the interfaces between the core and shell due to the shrinkage of ceramic fibers during calcination. The core-shell structure of the nanofiber is further confirmed by the TEM image, as shown in Fig. 8(c). The selected area electron diffraction (SAED) pattern in the inset of Fig. 8(c) confirms that both CFO and PZT phases exist in the nanofiber.

While routine PFM and magnetic hysteresis measurements have been carried out to confirm the multiferroic properties of core-shell nanofibers, we also developed a PFM based technique to demonstrate their magnetoelectric coupling. The schematic set up is shown in Fig. 9(a), where a variable magnetic field (VFM) module is used to apply an in-plane magnetic field up to 2000 Oe during PFM operation, making it possible to examine the change of PFM response of the nanofiber induced by magnetic field, as shown in Figs. 9(b)—(g). As clear in Figs. 9(b) and (d), after the application of external magnetic field, some initially disconnected domains are connected together, suggesting ferroelectric domain switching in PZT shell due to the applied magnetic field. Change in the magnitude of PFM amplitude is also observed, and the average amplitude of nanofiber decreases from 290.9 pm to 280.7 pm when the magnetic field is applied, as estimated from Figs. 9(c) and (e). The magnetoelectric coupling of the core-shell nanofiber is further confirmed by PFM switching characteristics before and after the application of magnetic field, as shown in Figs. 9(f) and (g). In fact, we can estimate lateral ME coefficient $\alpha_{31} = \Delta E_3/\Delta H_1$ from the butterfly loop, where ΔE_3 is the change in longitudinal electric field induced by the change in lateral magnetic field ΔH_1. Assuming that the piezoelectric constant d_{33} of the nanofiber does not vary with the magnetic field, the change in electric field can be evaluated from the change in piezoresponse displacement Δu as $\Delta E_3 = \Delta u/(d_{33}D)$, where D is the diameter of the nanofiber, and the piezoelectric coefficient d_{33} can be estimated from the butterfly loop as $d_{33} = u/V$ in the absence of the magnetic, where V is the applied AC voltage that induced piezoelectric vibration. All the data are read from the butterfly loop at remnant state where DC voltage is zero, with $\Delta u = 1.0$ nm and $u = 3.2$ nm, from which we estimate that $\alpha_{31} = 2.95 \times 10^4$ mV/(cm · Oe). This turns out to be two orders of magnitude higher than multiferroic thin films of similar composition [14], and confirms our theoretical analysis

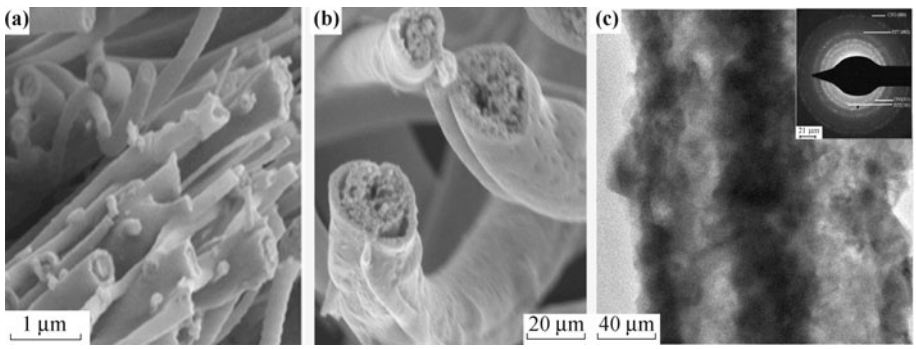

Fig. 8 The morphology of CFO-PZT core-shell nanofibers: **(a)** SEM overview of nanofibers; **(b)** cross-section SEM image; and **(c)** TEM image with SEAD pattern in inset. Reproduced from Ref. [34], Copyright © 2011 Royal Society of Chemistry.

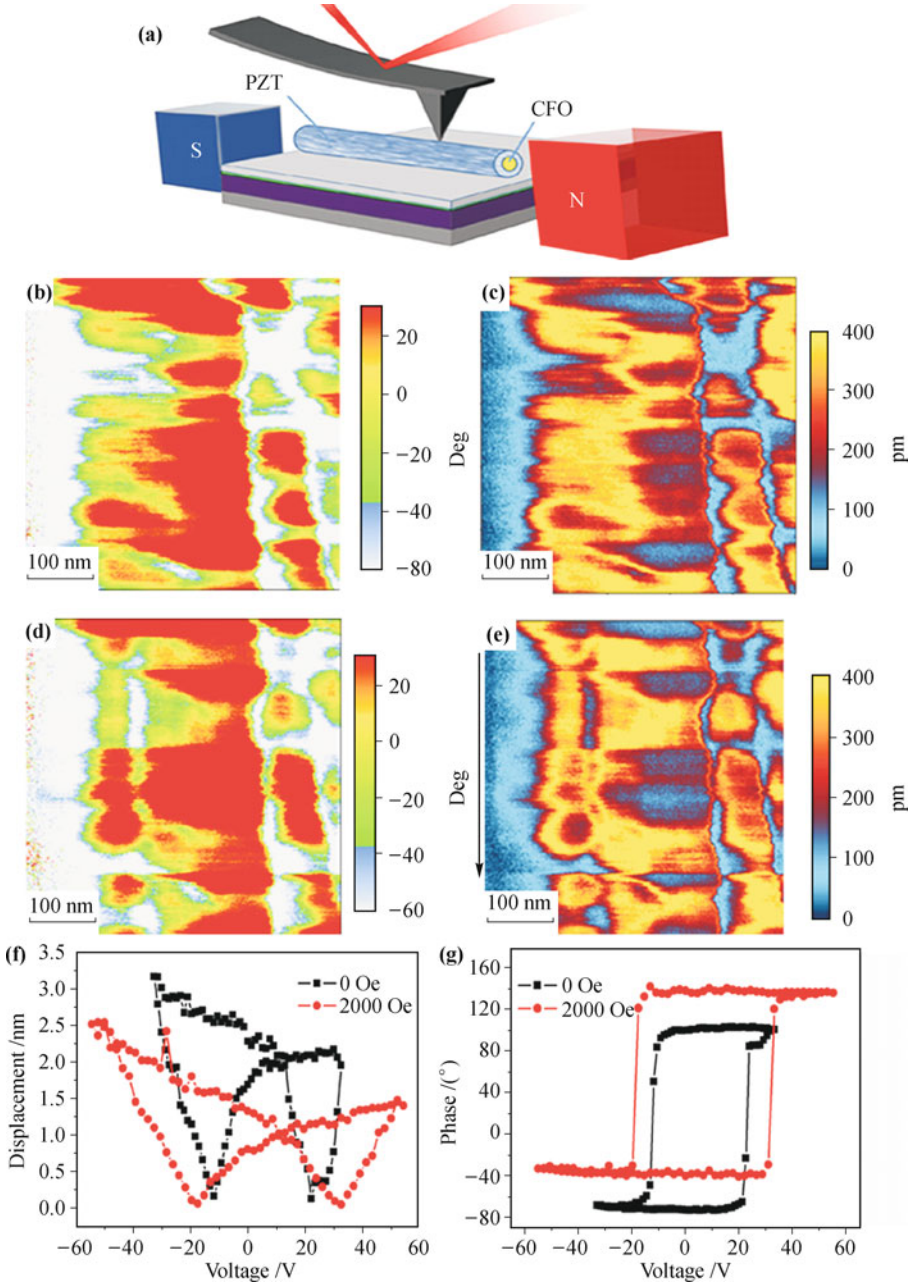

Fig. 9 The change of PFM response in a CFO-PZT core-shell nanofiber due to external magnetic field: **(a)** the schematic of SPM setup; **(b)** PFM phase and **(c)** amplitude of nanofiber without magnetic field; **(d)** PFM phase and **(e)** amplitude of nanofiber under 2000 Oe; and **(f)** PFM butterfly loop and **(g)** hysteresis loop with and without the magnetic field; the direction of magnetic field is indicated by the arrow. Reproduced from Ref. [34], Copyright © 2011 Royal Society of Chemistry.

presented in Section 2. The estimate, however, could be over-simplified, and further studies are underway.

5 Concluding remarks

In summary, the theoretical analysis suggested that multiferroic composite nanofibers possess higher magnetoelectric coupling than multiferroic composite thin film of similar compositions, and this motivated us to synthesize single-phase BFO nanofibers, PZT-CFO and PZT-NFO composite nanofibers, and CFO-PZT core-shell nanofibers using sol-gel based electrospinning. These nanofibers typically have diameters in the range of a few hundred nanometers and grain size in the range of 10s nanometers, and exhibits both ferroelectric and ferromagnetic properties. PFM based techniques have been developed to examine the magnetoelectric coupling of the nanofibers, as confirmed by the change of PFM response induced by external magnetic field. The magnetoelectric coefficient of the core-shell nanofibers is indeed estimated to be two orders of magnitude higher than that of thin films, consistent with our theoretical analysis.

The key challenge, however, remains to be the char-

acterizations of magnetoelectric coupling in multiferroic nanostructures, particularly in the aspect of quantitative analysis. Scanning probe microscopy based techniques provide powerful tools for such investigations, yet much more studies need to be carried out before definite conclusions can be drawn.

Acknowledgements We acknowledge the support of US National Science Foundation (DMR-1006194) and the National Natural Science Foundation of China (Grant Nos. 10772155, 10732100, 10972189, 10902095, and 11102175). S. H. Xie and Y. Y. Liu also acknowledge partial support of China Scholarship Council.

References

1. W. Eerenstein, N. D. Mathur, and J. F. Scott, Nature, 2006, 442(7104): 759
2. N. A. Spaldin and M. Fiebig, Science, 2005, 309(5733): 391
3. H. Zheng, J. Wang, S. E. Lofland, Z. Ma, L. Mohaddes-Ardabili, T. Zhao, L. Salamanca-Riba, S. R. Shinde, S. B. Ogale, F. Bai, D. Viehland, Y. Jia, D. G. Schlom, M. Wuttig, A. Roytburd, and R. Ramesh, Science, 2004, 303(5658): 661
4. N. Hur, S. Park, P. A. Sharma, J. S. Ahn, S. Guha, and S. W. Cheong, Nature, 2004, 429(6990): 392
5. M. Liu, O. Obi, J. Lou, Y. J. Chen, Z. H. Cai, S. Stoute, M. Espanol, M. Lew, X. D. Situ, K. S. Ziemer, V. G. Harris, and N. X. Sun, Adv. Funct. Mater., 2009, 19(11): 1826
6. Y. K. Fetisov and G. Srinivasan, Appl. Phys. Lett., 2006, 88(14): 143503
7. J. F. Scott, Nat. Mater., 2007, 6(4): 256
8. J. Y. Zhai, J. F. Li, S. X. Dong, D. Viehland, and M. I. Bichurin, J. Appl. Phys., 2006, 100(12): 124509
9. P. Yang, S. Peng, X. F. Wang, X. M. Lu, F. Yan, and J. S. Zhu, Appl. Phys. Lett., 2009, 94(8): 082904
10. R. Ramesh and N. A. Spaldin, Nat. Mater., 2007, 6(1): 21
11. J. Ma, Z. Shi, and C. W. Nan, Adv. Mater., 2007, 19(18): 2571
12. G. Srinivasan, E. T. Rasmussen, J. Gallegos, R. Srinivasan, Y. I. Bokhan, and V. M. Laletin, Phys. Rev. B, 2001, 64(21): 214408
13. T. K. Chung, G. P. Carman, and K. P. Mohanchandra, Appl. Phys. Lett., 2008, 92(11): 112509
14. J. G. Wan, X. W. Wang, Y. J. Wu, M. Zeng, Y. Wang, H. Jiang, W. Q. Zhou, G. H. Wang, and J. M. Liu, Appl. Phys. Lett., 2005, 86(12): 122501
15. S. Q. Ren, R. M. Briber, and M. Wuttig, Appl. Phys. Lett., 2009, 94(11): 113507
16. S. X. Dong, J. Y. Zhai, F. M. Bai, J. F. Li, D. Viehland, and T. A. Lograsso, J. Appl. Phys., 2005, 97(10): 103902
17. M. Liu, X. Li, J. Lou, S. Zheng, K. Du, and N. X. Sun, J. Appl. Phys., 2007, 102(8): 083911
18. J. M. Ding, C. G. Zhong, and Q. Jiang, Front. Phys., 2007, 2(3): 312
19. C. W. Nan, M. I. Bichurin, S. X. Dong, D. Viehland, and G. Srinivasan, J. Appl. Phys., 2008, 103(3): 031101
20. D. P. Dutta, O. D. Jayakumar, A. K. Tyagi, K. G. Girija, C. G. S. Pillai, and G. Sharma, Nanoscale, 2010, 2(7): 1149
21. H. C. He, J. Wang, J. P. Zhou, and C. W. Nan, Adv. Funct. Mater., 2007, 17(8): 1333
22. K. Raidongia, A. Nag, A. Sundaresan, and C. N. R. Rao, Appl. Phys. Lett., 2010, 97(6): 062904
23. P. Murugavel, M. P. Singh, W. Prellier, B. Mercey, Ch. Simon, and B. Raveau, J. Appl. Phys., 2005, 97(10): 103914
24. M. P. Singh, W. Prellier, C. Simon, and B. Raveau, Appl. Phys. Lett., 2005, 87(2): 022505
25. R. Ranjith, B. Kundys, and W. Prellier, Appl. Phys. Lett., 2007, 91(22): 222904
26. M. Liu, J. Lou, S. D. Li, and N. X. Sun, Adv. Funct. Mater., 2011, 21(13): 2593
27. N. Wang, J. Cheng, A. Pyatakov, A. K. Zvezdin, J. F. Li, L. E. Cross, and D. Viehland, Phys. Rev. B, 2005, 72(10): 104434
28. W. M. Zhu, H. Y. Guo, and Z. G. Ye, Phys. Rev. B, 2008, 78(1): 014401
29. J. R. Cheng, S. W. Yu, J. G. Chen, Z. Y. Meng, and L. E. Cross, Appl. Phys. Lett., 2006, 89(12): 122911
30. C. L. Zhang, W. Q. Chen, S. H. Xie, J. S. Yang, and J. Y. Li, Appl. Phys. Lett., 2009, 94(10): 102907
31. S. H. Xie, J. Y. Li, Y. Qiao, Y. Y. Liu, L. N. Lan, Y. C. Zhou, and S. T. Tan, Appl. Phys. Lett., 2008, 92(6): 062901
32. S. H. Xie, J. Y. Li, Y. Y. Liu, L. N. Lan, G. Jin, and Y. C. Zhou, J. Appl. Phys., 2008, 104(2): 024115
33. S. H. Xie, J. Y. Li, R. Proksch, Y. M. Liu, Y. C. Zhou, Y. Y. Liu, Y. Ou, L. N. Lan, and Y. Qiao, Appl. Phys. Lett., 2008, 93(22): 222904
34. S. H. Xie, F. Y. Ma, Y. M. Liu, and J. Y. Li, Nanoscale, 2011, DOI: 10.1039/C1NR10288E
35. C. J. Murphy and N. R. Jana, Adv. Mater. (Deerfield Beach Fla.), 2002, 14(1): 80
36. P. D. Markowitz, M. P. Zach, P. C. Gibbons, R. M. Penner, and W. E. Buhro, J. Am. Chem. Soc., 2001, 123(19): 4502
37. F. Gao, Y. Yuan, K. F. Wang, X. Y. Chen, F. Chen, J. Liu, and Z. F. Ren, Appl. Phys. Lett., 2006, 89: 2345825
38. B. A. Hernandez, K. S. Chang, E. R. Fisher, and P. K. Dorhout, Chem. Mater., 2002, 14(2): 480
39. N. Bao, L. Shen, G. Srinivasan, K. Yanagisawa, and A. Gupta, J. Phys. Chem. C, 2008, 112(23): 8634
40. C. Chen, J. R. Cheng, S. W. Yu, L. J. Che, and Z. Y. Meng, J. Crys. Grow., 2006, 291(1): 135
41. Q. H. Li, Y. X. Liang, Q. Wan, and T. H. Wang, Appl. Phys. Lett., 2004, 85(26): 6389
42. M. S. Park, G. X. Wang, Y. M. Kang, D. Wexler, S. X. Dou, and H. K. Liu, Angew. Chem., 2007, 119(5): 764
43. X. Zhu, Z. Liu, and N. Ming, J. Mater. Chem., 2010, 20(20): 4015
44. M. Liu, X. Li, H. Imrane, Y. J. Chen, T. Goodrich, Z. H. Cai, K. S. Ziemer, J. Y. Huang, and N. X. Sun, Appl. Phys. Lett., 2007, 90(15): 152501
45. D. Li, Y. Wang, and Y. N. Xia, Nano Lett., 2003, 3(8): 1167
46. X. H. Li, C. L. Shao, and Y. C. Liu, Langmuir, 2007, 23(22): 10920
47. Z. M. Huang, Y. Z. Zhang, M. Kotaki, and S. Ramakrishna, Compos. Sci. Technol., 2003, 63(15): 2223
48. S. A. Theron, E. Zussmana, and A. L. Yarin, Polymer, 2004, 45(6): 2017
49. R. Ramaseshan, S. Sundarrajan, R. Jose, and S. Ramakrishna, J. Appl. Phys., 2007, 102(11): 111101

50. X. L. Xu, X. L. Zhuang, X. S. Chen, X. R. Wang, L. X. Yang, and X. B. Jing, Macromol. Rapid Commun., 2006, 27(19): 1637
51. J. T. McCann, D. Li, and Y. N. Xia, J. Mater. Chem., 2005, 15(7): 735
52. J. Doshi and D. H. Reneker, J. Electrost., 1995, 35(2–3): 151
53. T. A. Kowalewski, S. Blonski, and S. Barral, Bull. Pol. Acad. Sci. Tech. Sci., 2005, 53: 385
54. S. Ramakrishna, K. Fujihara, W. E. Teo, T. Yong, Z. Ma, and R. Ramaseshan, Mater. Today, 2006, 9(3): 40
55. W. E. Teo and S. Ramakrishna, Nanotechnology, 2006, 17(14): R89
56. J. Lyons, C. Li, and F. Ko, Polymer, 2004, 45(22): 7597
57. D. Li and Y. N. Xia, Nano Lett., 2004, 4(5): 933
58. J. T. McCann, M. Marquez, and Y. N. Xia, Nano Lett., 2006, 6(12): 2868
59. J. Wang, J. B. Neaton, H. Zheng, V. Nagarajan, S. B. Ogale, B. Liu, D. Viehland, V. Vaithyanathan, D. G. Schlom, U. V. Waghmare, N. A. Spaldin, K. M. Rabe, M. Wuttig, and R. Ramesh, Science, 2003, 299(5613): 1719
60. T. J. Park, G. C. Papaefthymiou, A. J. Viescas, A. R. Moodenbaugh, and S. S. Wong, Nano Lett., 2007, 7(3): 766